Research Article

Hangyu Zhu*, Jixuan Zhao, Jianli Li*, Qian Hu, and Chenxi Peng

Evolution of nonmetallic inclusions in pipeline steel during LF and VD refining process

https://doi.org/10.1515/htmp-2020-0088
received April 29, 2020; accepted August 12, 2020

Abstract: The formation and evolution of nonmetallic inclusions in pipeline steel were investigated by SEM, EDS and INCA Feature Analysis System, with the industrial process of electric arc furnace → ladle furnace (LF) refining → vacuum degassing → continuous casting. The composition, size and amount of inclusions during refining process were discussed systematically. The results show that inclusions at each refining step are mainly small-particle inclusions (below 5 μm), and the total number of inclusions has been reduced significantly due to the refining effect of slag during LF refining. The calcium (Ca) treatment increases the amount of small inclusions. The types of inclusion are mainly Al_2O_3 and $MnO–SiO_2–Al_2O_3$ before LF, and they are transformed into $CaO–Al_2O_3$, $MgO–Al_2O_3$ and $CaO–MgO–Al_2O_3$ during LF process. After Ca treatment, inclusions are changed to $CaO–Al_2O_3$–(CaS) and $CaO–MgO–Al_2O_3$–(CaS). Typical inclusions are still mainly $CaO–Al_2O_3$ and $CaO–MgO–Al_2O_3$ in tundish, but the composition of those inclusions has been changed and located to the low melting point region in ternary phase diagram. Such inclusions will further be removed as continuous casting approaches.

Keywords: nonmetallic inclusion, pipeline steel, refining process, calcium treatment

* **Corresponding author: Hangyu Zhu,** The State Key Laboratory of Refractories and Metallurgy, Wuhan University of Science and Technology, Wuhan, 430081, China, e-mail: zhuhy@wust.edu.cn
* **Corresponding author: Jianli Li,** Key Laboratory for Ferrous Metallurgy and Resources Utilization of Ministry of Education, Wuhan University of Science and Technology, Wuhan, 430081, China, e-mail: jli@wust.edu.cn
Jixuan Zhao, Qian Hu, Chenxi Peng: Key Laboratory for Ferrous Metallurgy and Resources Utilization of Ministry of Education, Wuhan University of Science and Technology, Wuhan, 430081, China; Hubei Provincial Key Laboratory for New Processes of Ironmaking and Steelmaking, Wuhan University of Science and Technology, Wuhan, 430081, China

1 Introduction

Pipeline steels are usually used for the transportation of oil and natural gas over long distances under high pressure and require high strength, toughness, fatigue resistance and corrosion resistance. Nonmetallic inclusions directly affect the quality of pipeline steel [1–3]. Most of the researchers believe that noncoherent inclusions are considered as hydrogen-induced cracking (HIC)- initiation sites, and there is a strong correlation between HIC susceptibility, sulfur content, MnS and $CaO–Al_2O_3$ inclusions [4–6]. In our previous study, we have discussed the relationship between $CaO–Al_2O_3$, $MgO–Al_2O_3$ inclusions and inner fold and bulge defects; those brittle nonmetallic inclusions are the main causes of bulge and inner fold defects [7,8]. Moreover, nonmetallic inclusions will cause nozzle clogging and affect continuous casting (CC) process [9,10]. Therefore, the effective control of nonmetallic inclusions is very important for the production of pipeline steel.

The addition of Ca during refining process is a commonly used technique for the modification of MnS and Al_2O_3 inclusions and improvement of the steel cleanliness. Sidorova et al. [11] reported that $MgO–Al_2O_3$ and $SiO_2–Al_2O_3$ inclusions were modified to $CaO–MgO–Al_2O_3$ inclusions after Ca treatment, and the hot rolling process can change the number and composition of the corrosion-active nonmetallic inclusions. Hao et al. [12] and Li et al. [13] reported that the inclusions could be turned into $CaO–Al_2O_3$–CaS inclusions after Ca treatment, by changing the refining slag composition and Si–Ca wires during the LF process. Xu et al. [14] summarized two kinds of precipitation forms of CaS inclusion: one by the direct reaction of Ca and S and the other by the reaction of CaO in $CaO–Al_2O_3$ with dissolved Al and S in liquid steel. They also reported that the modification degree of Al_2O_3 inclusions had a great effect on the generation of CaS [15].

In the current study, the variation in the composition, size and amount of inclusions in pipeline steels produced by a 90 ton electric arc furnace (EAF) → ladle furnace (LF) refining → vacuum degassing (VD) → CC process was systematically investigated.

2 Materials and methods

2.1 Industrial process and sampling

The pipeline steel in the current study was produced by the process of 90 ton EAF → LF → VD → CC, and the steel samples were taken at each production step, as shown in Figure 1. About 40 ton scrap and 50 ton molten iron were smelted at EAF, and then the molten steel was tapped from the EAF into the ladle. The smelting time of EAF was 50–60 min, and the tapping temperature was about 1,625°C. During the tapping process, silicon manganese, silicon ferrosilicon and aluminum were added to the ladle for predeoxidization, then low-carbon ferrochromium, ferromolybdenum and ferroniobium were added for element alloying. At the same station, slag formers were added to form a synthetic slag. The ladle was then transferred to LF station, and deoxidization, desulfurization and adjusting composition of the molten steel were processed depending on the specification of the steel grade at this stage. After the target steel composition had been reached, the ladle was transferred to the VD station. During VD, the molten steel was stirred by argon gas to remove nitrogen, hydrogen and inclusion. The vacuum degree was 10 Pa, and the degassing time was about 15 min. After VD, Ca treatment was performed to modify inclusion. Then, the molten steel was transported to the CC platform for casting.

2.2 Analysis of samples

The steel samples (Φ 30 mm × 10 mm) were cleaned by machining the surface, and the chemical composition of pipeline steel in the current study is shown in Table 1. The contents of carbon and sulfur in steel samples were analyzed with a JF infrared absorption C/S instrument (CS-996), and the contents of nitrogen and oxygen in the steel samples were measured with a LECO Analyzer (TC-500).

Table 1: Chemical composition of pipeline steel in the current study (wt%)

C	Si	Mn	Cr	Mo	Nb	Ti	P	S
0.09	0.31	1.5	0.23	0.19	0.02	0.018	0.013	0.003

The 15 mm × 15 mm × 10 mm samples for the scanning electron microscopy (SEM, ZEISS ASIN EVO10, Carl Zeiss Microscopy Ltd, Germany) were made by cutting, grinding and polishing. The composition of nonmetallic inclusions of the steel specimens was detected by the energy-dispersive spectrometer (EDS, X-Max 80, Oxford Instruments, High Wycombe, UK). Inclusions in the current steel samples were analyzed using INCA Feature Analysis System for their two-dimensional morphology, size and composition. In the current study, only inclusions larger than 1 μm are considered.

3 Results and discussion

3.1 Changes of oxygen and nitrogen contents

The O and N contents of the steel samples from different refining steps in this study are shown in Figure 2. During LF refining, the O content decreases from 42.98 to 27.95 ppm, before LF refining is 42.98 ppm, due to the deoxidization reaction with aluminum, silicon manganese and ferrosilicon. After VD, the O content is reduced to 15.72 ppm due to argon blowing and vacuum degassing treatment, which is conducive to the flotation of

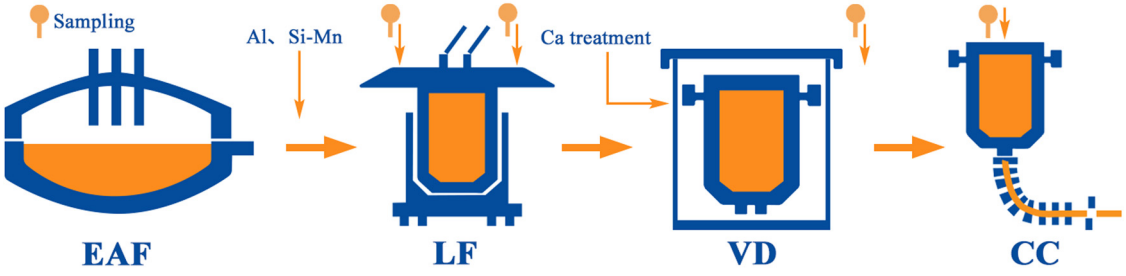

Figure 1: Steel-making process and sampling location in the current study.

inclusions and precipitation of dissolved oxygen in the molten steel. The content of oxygen in the steel sample from tundish increases slightly to 17.23 ppm due to secondary oxidation during the transportation of ladle and casting process.

The N content in the molten steel is generally on the rise during refining process. As a note, the N content decreases from 44.78 to 42.5 ppm during VD process due to the precipitation of dissolved nitrogen in the molten steel under vacuum. The nitrogen content will continue to decrease with the increase in vacuum holding time. When the liquid steel is transferred to tundish, the N content increases significantly to 45.75 ppm due to liquid steel reacting with air during the ladle transportation and casting process.

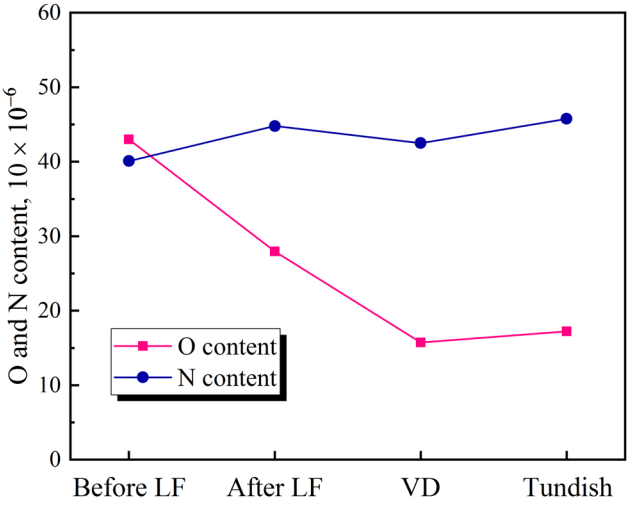

Figure 2: Changes of oxygen and nitrogen contents during refining process.

3.2 Composition of inclusions in refining process

INCA Feature Software is used to analyze the composition and size distribution of inclusions from different refining steps, and the scanning area is 2 × 3 mm. The elements such as Al, Mg, Ca, Si and Mn in inclusions were normalized and converted into various types of oxidation, and then the inclusion composition was mapped to ternary phase diagram for further analysis, as shown in Figure 3. Red line represents the liquidus of 1,600°C by considering ternary phase diagram and the blue line represents the liquidus of 1,500°C.

The inclusions before the LF treatment mainly consist of Al_2O_3, MnO and SiO_2. A small amount of large CaO inclusions are detected, and no MgO inclusions are detected. As shown in Figure 3(a), it can be seen from the $CaO–Al_2O_3–SiO_2$ phase diagram that there are many aluminosilicate inclusions, which are not located to the low melting point region. Moreover, for the $Al_2O_3–SiO_2–MnO$ ternary phase diagram, there are many Al–Si–Mn composite inclusions, and many small-particle composite inclusions are located in the low melting point region, which will be effectively removed during LF refining.

After LF refining, MnO inclusions are significantly reduced, only with few small size MnO inclusions due to the reaction of MnO inclusions and SiO_2 from refining slag. On the contrary, the number of $CaO–Al_2O_3$, $MgO–Al_2O_3$ and $CaO–MgO–Al_2O_3$ inclusions increases. It can be seen from Figure 3(b) that $CaO–Al_2O_3$ and $CaO–MgO–Al_2O_3$ inclusions have larger size, but fortunately, these are located in the low melting point region and those inclusions will be removed by floating to the top slag in the subsequent refining processes. In addition, inclusions containing SiO_2 decrease in this stage due to the interfacial reaction between CaO (slag) and SiO_2 (inclusion), and the formed calcium silicate inclusions may be captured by the refining slag.

After VD treatment, as shown in Figure 3(c), almost no MnO-containing inclusions are found. Al_2O_3-Containing inclusions are significantly reduced due to Ca treatment. The main inclusions are still $CaO–Al_2O_3$-type inclusions, and the small-particle inclusions increase. A large amount of $CaO–MgO–Al_2O_3$ inclusions are still outside the low melting point region, because of the rise in MgO content in inclusions.

For the steel sample from tundish, its quality improves significantly, as shown in Figure 3(d). There are few SiO_2 type inclusions, and no MnO-containing inclusions are found. The detected inclusions are $CaO–Al_2O_3$ and $CaO–MgO–Al_2O_3$, which are located in the low melting point region. Those inclusions will further be removed during the tundish casting process.

3.3 Morphology of inclusions during refining process

The typical Al_2O_3 and Al–Si–Mn composite inclusions before the LF treatment are shown in Figure 4. A large number of Al_2O_3 inclusions with small size are observed, generally about 2 μm. In addition, partical Al_2O_3 inclusions

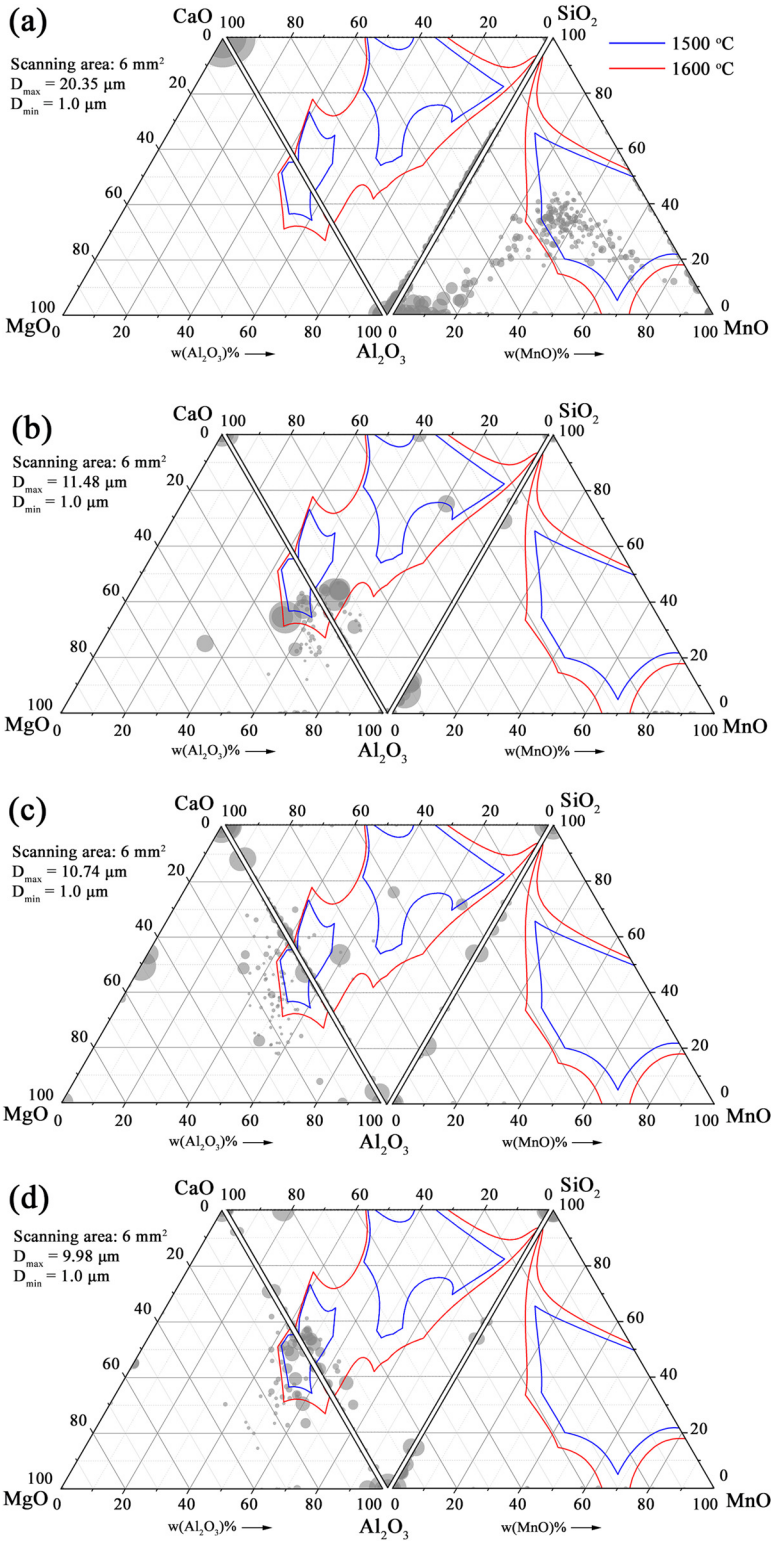

Figure 3: Composition distributions of inclusions in steel samples at different refining stages: (a) before LF, (b) after LF, (c) after VD and (d) tundish.

are wrapped up with MnS. The size of typical Al–Si–Mn composite inclusions are up to 20 μm, which consist of Al_2O_3 and MnO–SiO_2. The formation reason of the above-mentioned inclusions is that the molten steel is deoxidized by aluminum and silicon-manganese alloys during tapping process, and the inclusions are mainly endogenous.

During the LF treatment, high basicity refining slag is used to desulfurize. The refining slag is composed of CaO, Al_2O_3 and MgO, which will modify the composition of inclusion in the molten steel. Typical inclusions after LF treatment are CaO–Al_2O_3 and CaO–MgO–Al_2O_3, with a size of about 5 μm, as shown in Figure 5. The formation mechanism of CaO–Al_2O_3 and CaO–MgO–Al_2O_3 is aluminum reacting with MgO and CaO from slag, as shown in equations (1)–(5) [12,13].

$$2[Al] + 3(MgO)_{slag} = 3[Mg] + (Al_2O_3)_{slag} \quad (1)$$

$$[Mg] + n/3(Al_2O_3)_{inclusion} = (MgO \cdot (n-1)/3Al_2O_3)_{inclusion} + 2/3[Al] \quad (2)$$

$$2[Al] + 3(CaO)_{slag} = 3[Ca] + (Al_2O_3)_{slag} \quad (3)$$

$$x[Ca] + (yMgO \cdot zAl_2O_3)_{inclusion} = (xCaO \cdot (y-x)MgO \cdot zAl_2O_3)_{inclusion} + x[Mg] \quad (4)$$

$$x[Ca] + (y + x/3)(Al_2O_3)_{inclusion} = (xCaO \cdot yAl_2O_3)_{inclusion} + 2x/3[Al] \quad (5)$$

After VD, the Ca-containing inclusions increase significantly due to Ca treatment. It is mainly spherical endogenous inclusion, and there are also a large number of composite inclusions wrapped up with CaS. Figure 6(a) shows the nearly spherical CaO–Al_2O_3 inclusion, and Figure 6(b) and (c) show the typical CaO–MgO–Al_2O_3 composite inclusion covered with CaS inclusion. Equations (6)–(9) indicate that calcium reacts with MgO and Al_2O_3 inclusions in the molten steel, resulting in Ca-containing inclusions increase and MgO and Al_2O_3 inclusions decrease [12,13]. Moreover, calcium reacts with sulfur in the molten steel to form CaS inclusion.

$$[Ca] + (MgO)_{inclusion} = [Mg] + (CaO)_{inclusion} \quad (6)$$

$$[Ca] + (Al_2O_3)_{inclusion} = 2[Al] + 3(CaO)_{inclusion} \quad (7)$$

$$[Ca] + [S] = (CaS)_{inclusion} \quad (8)$$

$$2[Al] + 3[S] + 3(CaO)_{inclusion} = 3(CaS)_{inclusion} + (Al_2O_3)_{inclusion} \quad (9)$$

For the steel sample from tundish, the inclusion type is similar to that from VD stage, as shown in Figure 7. The only difference is that the content of CaS decreases, and the number of CaS-containing inclusions is lower. During the transfer of ladle to tundish step, the number of inclusions in the molten steel is significantly reduced, and further reaction of inclusions in the molten steel occurred. Inclusion composition has significantly been changed comparing with the steel sample from the VD step, and they all aggregated into the low melting point regions of CaO–Al_2O_3–MgO and CaO–Al_2O_3–SiO_2 phase diagrams, as shown in Figure 3(d). Such inclusions can be further reduced as time approaches.

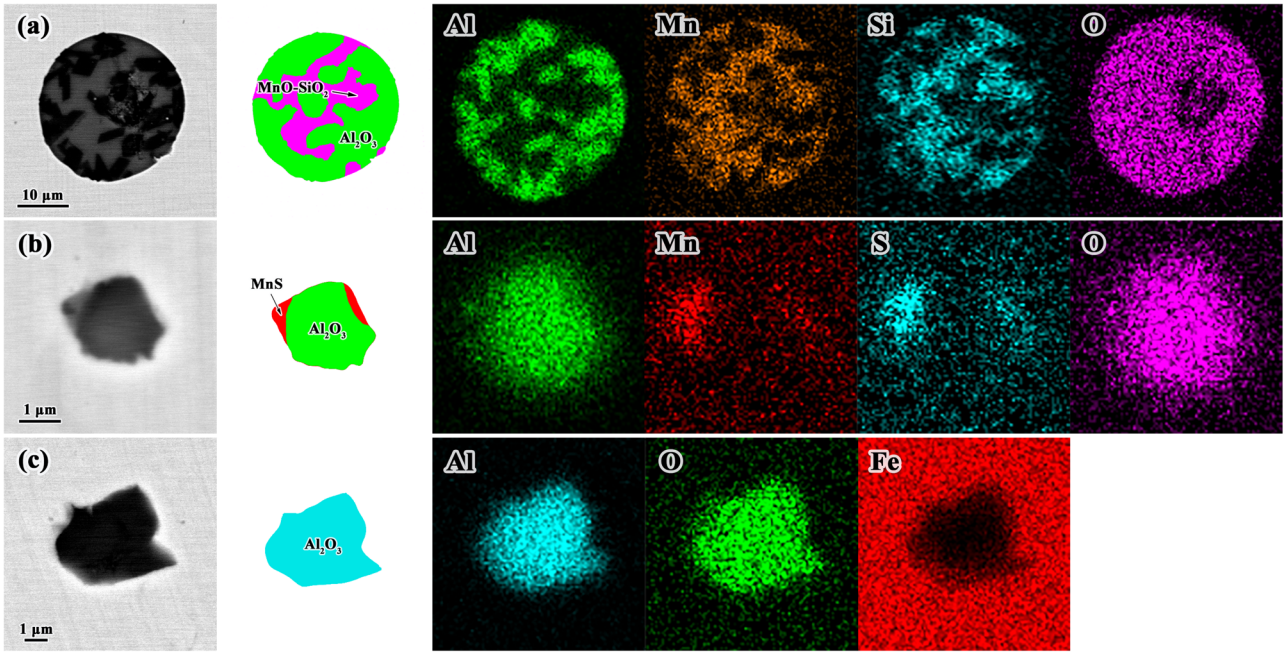

Figure 4: Element mapping of typical inclusions in steel samples before LF treatment. (a) MnO–SiO_2–Al_2O_3, (b) Al_2O_3–MnS and (c) Al_2O_3.

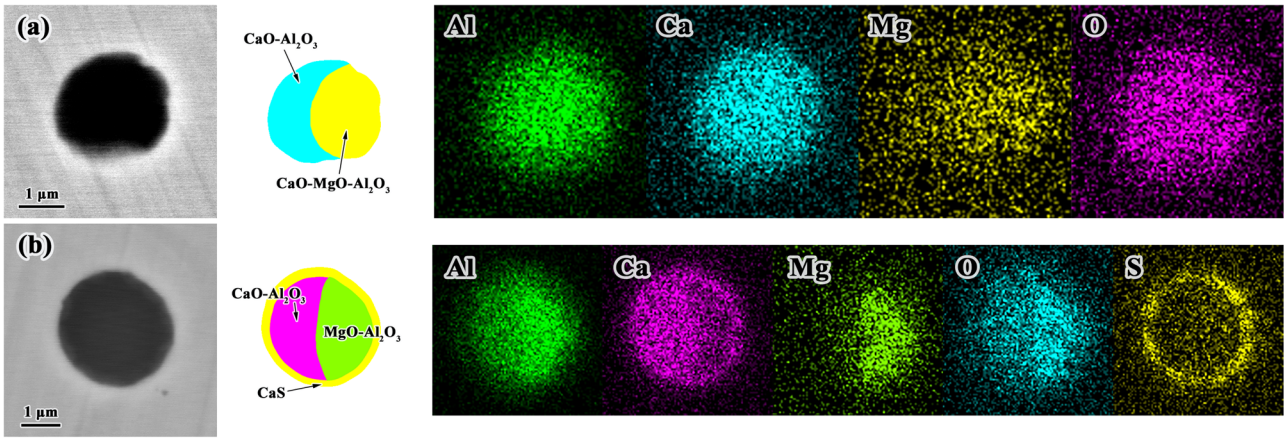

Figure 5: Typical inclusions in steel samples after LF refining: (a) $CaO–MgO–Al_2O_3$, (b) $CaO–Al_2O_3$ and $MgO–Al_2O_3$.

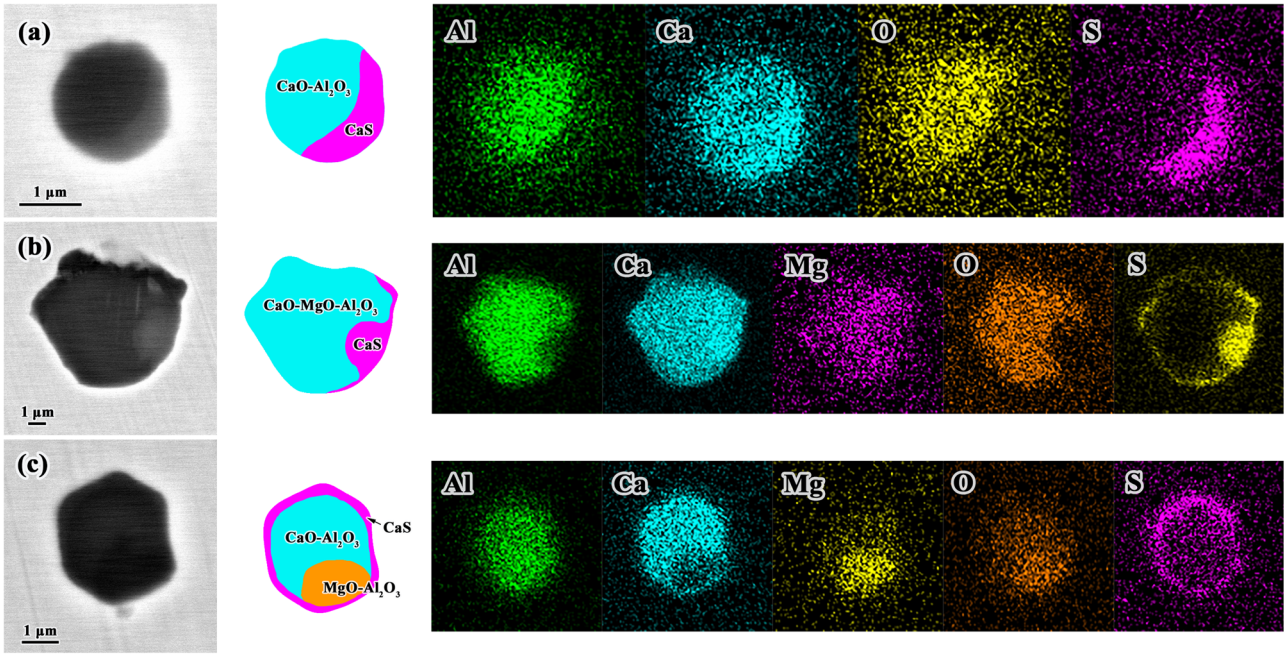

Figure 6: Typical inclusions in steel samples after vacuum degassing: (a) $CaO–Al_2O_3–CaS$, (b) and (c) $CaO–MgO–Al_2O_3–CaS$.

3.4 Size distribution of inclusions

It can be seen that inclusions at each refining station are mainly small-particle inclusions below 2 μm, followed by 2–5 μm inclusions, as shown in Figure 8. Before the LF treatment, the number of inclusions is larger, with size of 1–2 μm and 2–5 μm, which is 302 and 150 separately. After LF refining, the total number of inclusions is reduced due to the refining effect of slag. The Ca treatment after VD increases the number of small-particle inclusions with the composition of CaS. The tundish molten steel has higher cleanliness, and the number of inclusions is significantly reduced. No inclusions larger than 10 μm are detected.

3.5 Inclusion variation during refining process

The inclusion evolution behavior of the current pipeline steel during refining process is shown in Figure 9. Before the LF treatment, the inclusions are mainly Al_2O_3 and $MnO–SiO_2–Al_2O_3$. After LF refining, the SiO_2 and MnO

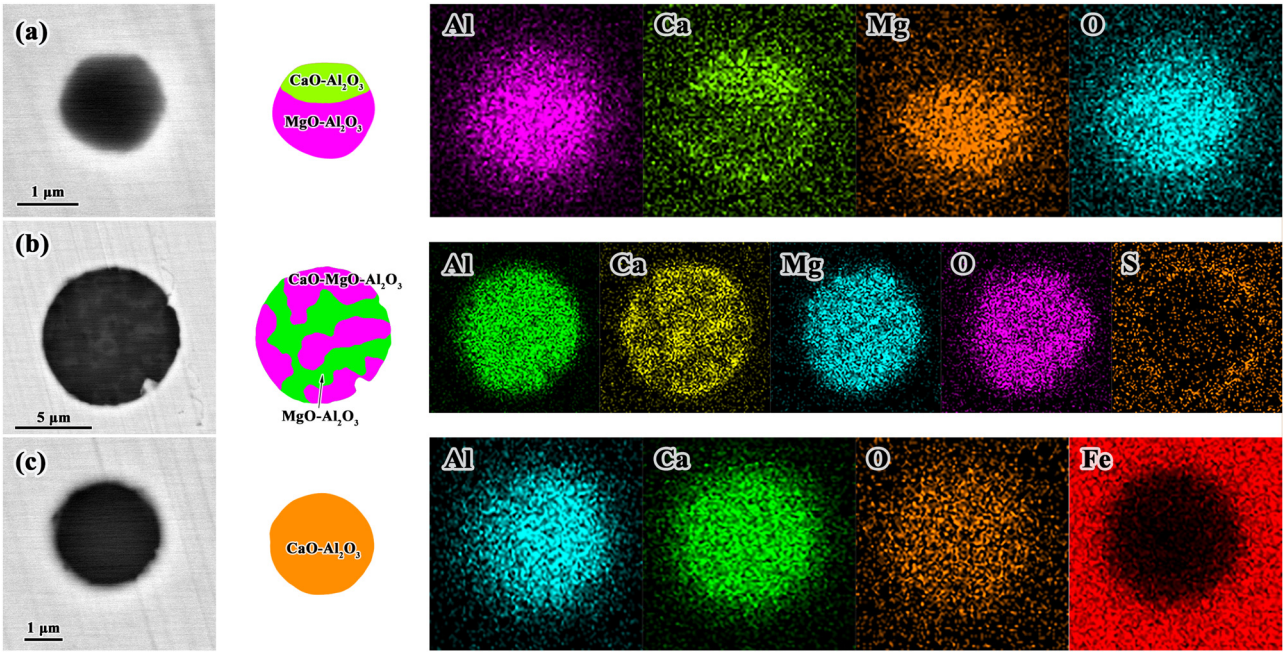

Figure 7: Element mapping of typical inclusions in the tundish: (a) $MgO–Al_2O_3$, (b) $CaO–MgO–Al_2O_3$ and (c) $CaO–Al_2O_3$.

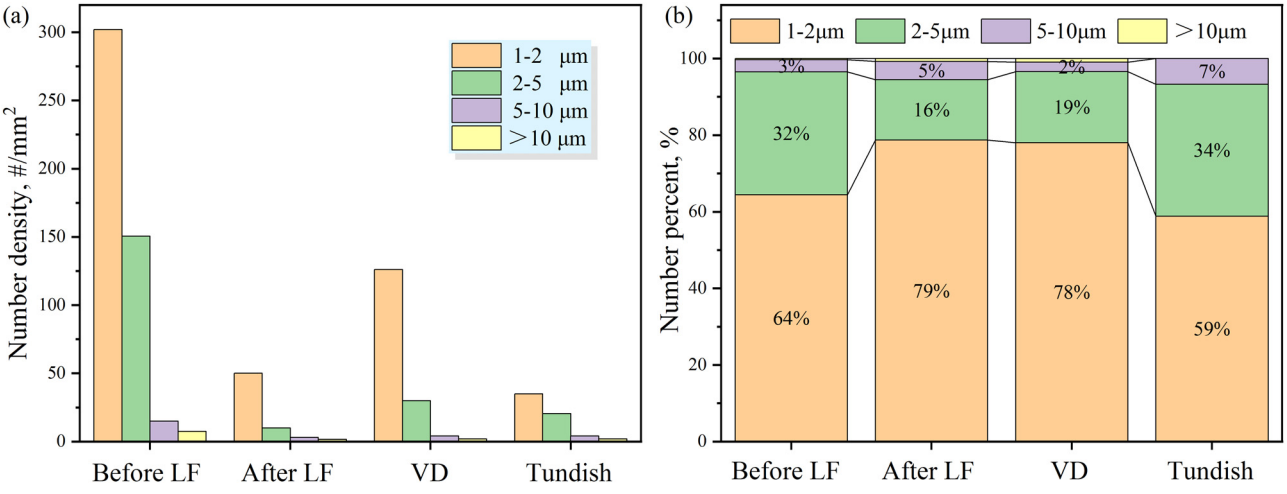

Figure 8: Size distribution of inclusions during refining process: (a) inclusion counts and (b) number percent.

inclusions are significantly reduced under the action of the refining slag. Al_2O_3 inclusions in the molten steel are transformed into $CaO–Al_2O_3$, $MgO–Al_2O_3$ and a small amount of $CaO–MgO–Al_2O_3$ composite oxides due to the dissolved aluminum in steel reacting with MgO and CaO from slag. Although the $CaO–MgO–Al_2O_3$ composite inclusions are relatively larger in size, they are all located in the low melting region and will float to slag in the subsequent refining process. For inclusions in the steel sample from VD with Ca treatment, they are transformed into $CaO–Al_2O_3–(CaS)$ and $CaO–MgO–Al_2O_3–(CaS)$. The reason is that calcium is difficult to diffuse in a short time, and the local calcium content in the molten steel is high, which leads to the formation of CaS inclusions. As the ladle is transferred to turret, the typical inclusions are still mainly $CaO–Al_2O_3$ and $CaO–MgO–Al_2O_3$; however, composition of inclusions has been changed and is closer to the low melting point region in ternary phase diagram. These inclusions are further removed during the casting process.

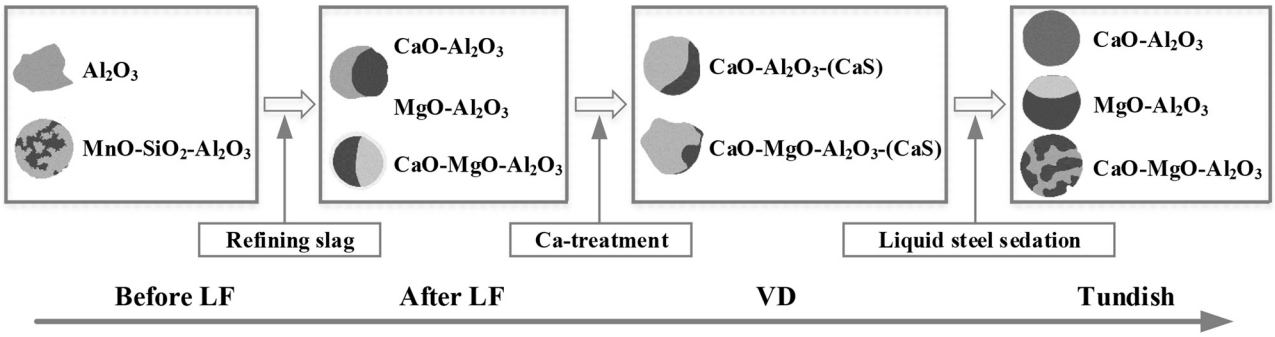

Figure 9: Inclusion evolution behavior during refining process.

4 Conclusions

In the current study, the characteristics and the evolution behavior of nonmetallic inclusion in pipeline steel during refining process are systematically investigated by micro-analysis. Final conclusions from this work are as follows:

(1) The O content generally decreases during refining process, and its content increases slightly from 15.75 ppm to 17.23 ppm, due to secondary oxidation during the transportation of ladle and casting process. VD decreases N content from 44.78 ppm to 42.5 ppm, and its content increases to 45.75 in tundish with a reason of reoxidation.

(2) Inclusions at each refining step are mainly small-particle inclusions below 2 μm, followed by 2–5 μm. The total number of inclusions is reduced significantly due to the refining effect of slag during LF refining. The Ca treatment increases the amount of small-particle inclusion. The molten steel in tundish has higher cleanliness.

(3) Inclusions are mainly Al_2O_3 and $MnO–SiO_2–Al_2O_3$ before LF, which will be transformed into $CaO–Al_2O_3$, $MgO–Al_2O_3$ and $CaO–MgO–Al_2O_3$ composite oxides during the LF process. Inclusions are changed to $CaO–Al_2O_3–(CaS)$ and $CaO–MgO–Al_2O_3–(CaS)$ due to Ca treatment. Typical inclusions are still mainly $CaO–Al_2O_3$ and $CaO–MgO–Al_2O_3$ in tundish, but the composition of those inclusions has been changed and is located in the low melting point region in ternary phase diagram. Such inclusions will further be removed as time approaches.

Acknowledgments: This work was supported by the National Natural Science Foundation of China (Grant No. 51604198 and 51974210). The authors would like to thank the engineers at Hengyang Steel Tube for their efforts in helping to perform this research.

References

[1] Xue, H. B., and Y. F. Cheng. Characterization of inclusions of X80 pipeline steel and its correlation with hydrogen-induced cracking. *Corrosion Science*, Vol. 53, No. 4, 2011, pp. 1201–1208.

[2] Huang, F., J. Liu, Z. Y. Deng, J. H. Cheng, Z. H. Lu, and X. G. Li. Effect of microstructure and inclusions on hydrogen induced cracking susceptibility and hydrogen trapping efficiency of X120 pipeline steel. *Materials Science and Engineering: A*, Vol. 527, No. 26, 2010, pp. 6997–7001.

[3] Kim, W. K., S. U. Koh, B. Y. Yang, and K. Y. Kim. Effect of environmental and metallurgical factors on hydrogen induced cracking of HSLA steels. *Corrosion Science*, Vol. 50, No. 12, 2008, pp. 3336–3342.

[4] Liu, Z. Y., X. G. Li, C. W. Du, L. Lu, Y. R. Zhang, and Y. F. Cheng. Effect of inclusions on initiation of stress corrosion cracks in X70 pipeline steel in an acidic soil environment. *Corrosion Science*, Vol. 51, No. 4, 2009, pp. 895–900.

[5] Maiti, R., and E. B. Hawbolt. The effect of inclusion parameters on the fracture toughness of two X-70 Pipeline steels. *Journal of Materials for Energy Systems*, Vol. 6, No. 4, 1985, pp. 242–250.

[6] Dong, C. F., Z. Y. Liu, X. G. Li, and Y. F. Cheng. Effects of hydrogen-charging on the susceptibility of X100 pipeline steel to hydrogen-induced cracking. *International Journal of Hydrogen Energy*, Vol. 34, No. 24, 2009, pp. 9879–9884.

[7] Li, B.S., H. Y. Zhu, Z. L. Xue, Z. F. Qin, and J. Sun. Analysis of inner fold and bulge defects on J55 steel for oil casing pipe. *AIP Advance*, Vol. 9, No. 8, 2019, id. 085109.

[8] Zhu, H. Y., L. Q. Wang, J. L. Li, J. X. Zhao, and Y. Yu. Effects of metallurgical factors on reticular crack formations in Nb-bearing pipeline steel. *High Temperature Materials and Processes*, Vol. 39, 2020, pp. 81–87.

[9] Yang, L. L., Y. P. Bao, and J. H. Liu. Investigations in non-metallic inclusions modification effects of calcium treatment in steel. *Steelmaking*, Vol. 25, No. 4, 2009, pp. 35–38.

[10] Sun, Y. H., X. S. Wang, Z. B. Xu, K. K. Cai, C. F. Wang, and L. T. Liu. Thermodynamics of calcium treatment on high-alumina steel. *Journal of University of Science and Technology Beijing*, Vol. 33, No. s1, 2011, pp. 121–125.

[11] Sidorova, E., A. V. Karasev, D. Kuznetsov, and P. G. Jönsson. Modification of non-metallic inclusions in oil-pipeline steels by Ca-treatment. *Metals*, Vol. 9, No. 4, 2019, id. 391.
[12] Hao, X., Z. Y. Chen, X. Y. Bai, H. Y. An, and J. X. Chen. Study on control of B-type inclusion in high grade pipeline steel. *Steelmaking*, Vol. 35, No. 3, 2019, pp. 74–78.
[13] Li, Q., J. Q. Zhao, X. F. Cai, and C. D. Zou. Optimization of calcium treatment process for pipeline steel. *Steelmaking*, Vol. 35, No. 5, 2019, pp. 37–42.
[14] Xu, G., Z. H. Jiang, and Y. Li. Formation mechanism of CaS-bearing inclusions and the rolling deformation in Al-lilled, low-alloy steel with Ca treatment. *Metallurgical and Materials Transactions: B*, Vol. 47, No. 8, 2016, pp. 2411–2420.
[15] Xu, G., Z. H. Jiang, Y. Li, and C. Zhang. Study of CaS formation mechanism in X80 pipeline steel. *Journal of Northeastern University*, Vol. 38, No. 1, 2017, pp. 62–66.